High-Speed Traveling-Wave Electroabsorption Modulators

Yi-Jen Chiu, Sheng Z. Zhang,[a] Volkan Kaman,[b] Joachim Piprek, and John E. Bowers

Department of Electrical and Computer Engineering

University of California at Santa Barbara, Santa Barbara, CA 93106

[a] currently with Zaffire Inc., [b] currently with Calient Networks Inc.

ABSTRACT

Electroabsorption modulators (EAMs) based on the quantum confined Stark effect in multiple quantum wells (MQWs) have advantages for high-speed, low drive voltage, and high extinction ratio applications. In this paper, a traveling-wave electrode structure is proposed to achieve high bandwidths with long devices and lower drive voltages at 1.55μm wavelength. An InGaAsP/InGaAsP MQW traveling-wave electroabsorption modulator (TWEAM) with a bandwidth above 20 GHz is fabricated. A drive voltage of 1.2 V for an extinction ratio of 20-dB is demonstrated. The effects of microwave transmission on the high-speed performance of TWEAMs are discussed. Successful data transmission experiments at 30 Gbit/s show a promising system performance of these devices. By using an integrated tandem TWEAM, pulse data transmission above 100 Gbit/s is achieved.

Keywords: electroabsorption modulator, quantum confined Stark effect, traveling wave design, microwave transmission, high-speed modulation, InGaAsP.

1. INTRODUCTION

External optical modulators are very important for optical fiber communication with high-speed modulation in digital and analog systems. Using quantum-confined-Stark (QCS) effects, InP-based electroabsorption modulators (EAM) have attracted a lot of interests due to the capability of integrating with lasers, intrinsic low chirp and high extinction ratios operation. Figure 1 shows the quantum well under the perpendicular electric field which causes a red-shifted optical absorption so that the optical transmission in the waveguide can be modulated. To reduce the driving voltage of modulation, it is essential to optimize the parameters, such as the bandgap and well thickness of the MQW absorption layer. Because of the quadratic relation of the energy shift to the electric field (shown in figure 1) [1], it is necessary to make the unintentionally doped region thinner to increase the electric field. However, the reduction in the intrinsic layer thickness will reduce the bandwidth for a lumped device in the same proportion. It was verified that increasing the well thickness leads to a larger QCSS and a lower driving voltage, while decreasing in the oscillation strength of the electroabsorption [2, 3]. There is thus an optimum well thickness for high modulation efficiency. Simulation has shown that the optimum well thickness is around 8-9 nm to achieve the highest contrast ratio [4].

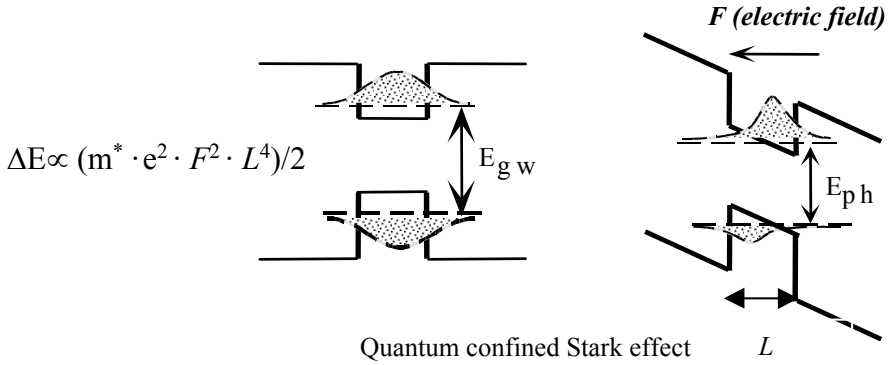

Figure 1. Red shift of quantum well energy level due to quantum-confined-Stark (QCS) effect. ΔE : energy level shift. *F*: electric field strength. *L* : quantum well thickness.

In the high frequency performance, conventional lump-EAMs needed to be short to obtain high-speed due to the total capacitance [5]. However, it inevitably trade-offs the modulation efficiency and the extinction ratio. The tolerance of material design is thus restricted. Traveling-wave EAMs (TWEAM) are proposed to overcome the RC-lump limitation for longer devices [6,7], therefore high extinction ratio and saturation power can be achieved. Figure 2 shows the schematic diagrams of lump and traveling-wave EAMs. In the lump configuration, the microwave signal is applied to the center of waveguide. At high frequency, a lump-type behavior will be induced due to the strong microwave reflections on both ends, i.e. the device speed is dependent on the total RC time constant. As shown in figure2a, the modulator can be modeled as p-i-n junction capacitance (C_i) and and the differential resistance (R_d), where the electroabsorption effect is generated from the intrinsic region (C_i), and R_d represents the resistivity of p- and n- semiconductor materials and metal contact. As operated in lump type, the modulation efficiency can be improved by increasing the device length, however, the device junction capacitance will degrade the high frequency performance. To avoid such RC-lump limitation, the traveling wave configuration is designed to have microwave co-propagate with optical waves. By matching the output termination, the electro-optic conversion is dominated by the distributed interaction between microwave and optical wave. As described in transmission line, as shown in figure 3(b), the microwave experiences distributed junction-capacitance and inductance along the waveguide, thus the limitation is not the total capacitance, rather the microwave characteristics, termination and the velocity.

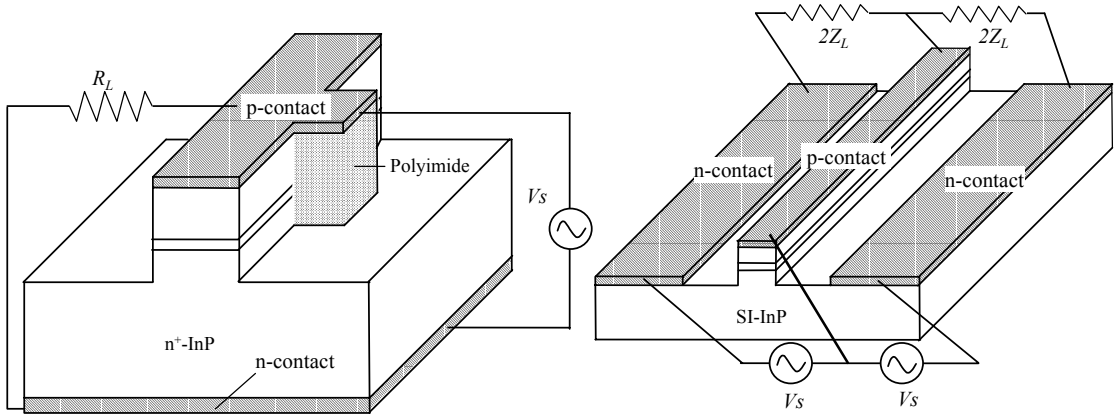

Figure 2. Schematic diagrams of lump type (left) and traveling-wave type (right) electroabsorption modulators.

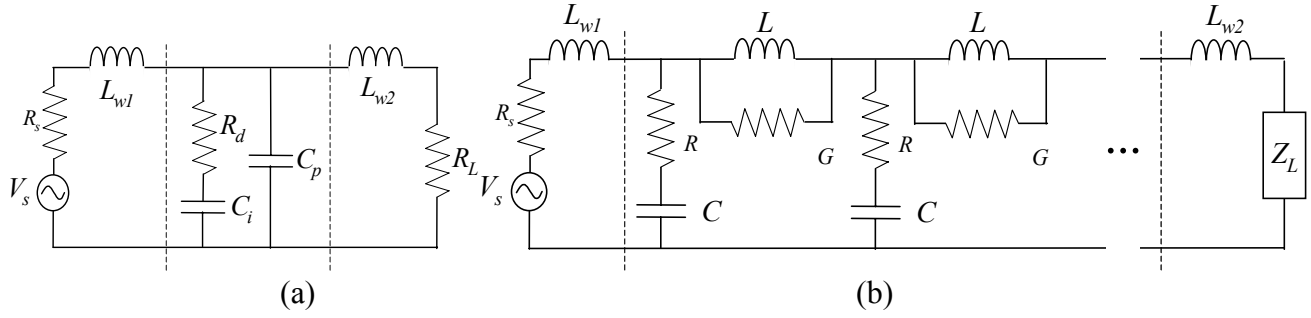

Figure 3. (a) Equivalent circuit model of lump type device (left of figure 2). (b) Distributed model of traveling-wave type modulator (right of figure 2). L_w : inductor of wire bond. R_s : source resistance. C_p : contact pad capacitance. R_L : output loaded impedance.

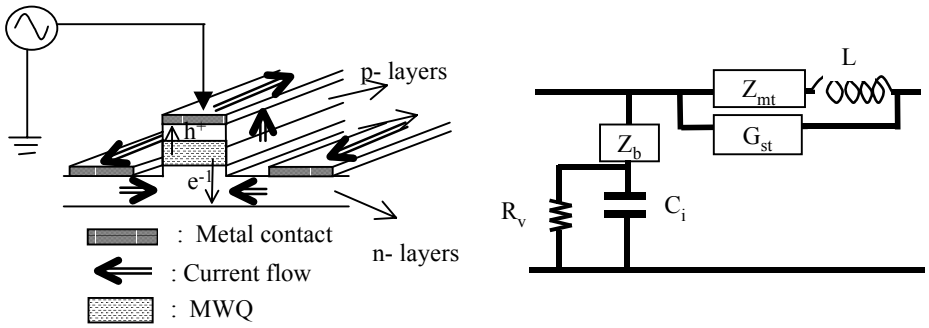

Figure 4. Schematic diagrams of waveguide and the corresponding equivalent circuit model.

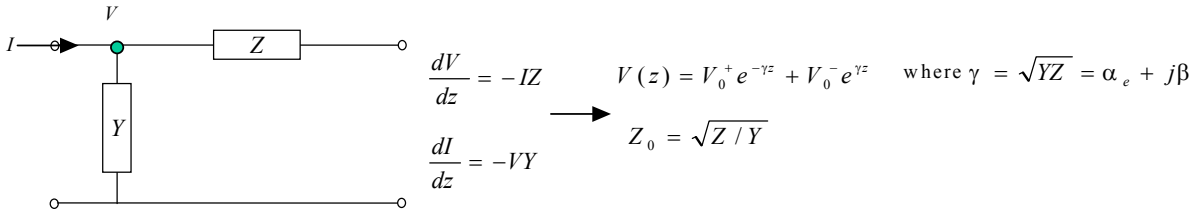

Figure 5. General transmission line circuit model. The microwave can be calculated by forward and backward wave with dispersion (β) and loss (α). α_e : microwave attenuation. β (=ω/v_e) *:* microwave wavenumber. Z_0 *:* characteristic impedance.

2. MICROWAVE DESIGN AND DISTRIBUTED EA-MODULATION

2.1 Microwave design

As described in the introduction, to optimize the device performance of the traveling wave type electrode, it is essential to know the microwave characteristics and velocity mismatch from the optical wave. Figure4 shows the cross section of the optical waveguide. The optical absorption region is a multiple-quantum-wells region (intrinsic), which is sandwiched by n- and p- doped cladding layers. As electrical signal is sent to such kind of waveguide, the generated microwave will have propagation characteristics of both CPW and microstrip lines (shown in the current flow of figure 4). The currents are primarily carried in the metal conductors and nearly all of the voltage drops across the insulator layer. Thus, the magnetic field distribution is similar as CPW lines, while the electric field pattern is similar to that of a microstrip structure. The equivalent circuit model can be described as shown in figure4 (right side), which has been examined by the full wave analysis [8]. C_i is the intrinsic capacitance from the MQW, which is proportion to the waveguide width divided by the thickness of intrinsic region. R_v is the resistance from the voltage-controlled current. Z_{mt} is the metal impedance, which is from the metal skin-effect at high frequency. L is the metal inductance. G_{st} is the conductance of semiconductor in the longitudinal direction, which is mainly from the non-TEM microwave. The transverse impedance, Z_b, is composed of the transverse impedance from the p-contact layer, p-cladding layer and n-cladding layer, the spreading resistance under the ridge, the bulk resistance of the gap, and the resistance of the ground contact.

Using the equivalent circuit model, the microwave propagation can be calculated by the transmission line theory, as shown in figure 5. Compared with the CPW line (figure 4) of the same dimensions, the hybrid-CPW and microstrip lines have a higher intrinsic capacitance, the electric field is almost confined in the thin intrinsic region. Therefore, with high frequency, the electric flow will cross the resistive n- and p- doped layers and microwave propagation will experience higher field attenuation. One more major factor effecting the microwave characteristics originates from the metal impedance (Z_{mt}) and inductance (L) with the semiconductor conductivity (G_{st}). Reducing the capacitance by decreasing the width will increase the metal impedance and inductance. Generally, if the metal is much thicker than 0.4μm, the skin effects can be neglected up to 40GHz (skin depth ~0.4μm for Au). Also, the microwave transmission is operated in the quasi-TEM mode, so the finite conductance G_{st} is quite small. The microwave loss is dominated by the highly loaded capacitance. To furthermore examine this effects for the design of high speed TWEAM, a 2μm Au metal is chosen to calculate the characteristics. As shown in figure 6, the trend is that reducing the loaded capacitance could improve the electrical loss. Figure 7 shows the calculated impedance as function of the ridge width and the intrinsic regions. Decreasing the intrinsic

capacitance can increase the characteristic impedance. Hence, to improve the propagation and impedance matching to 50Ω, the loaded capacitance should be reduced. Considering the optical coupling into the waveguide and the diffraction limitation of 1550nm light, 2μm wide device is chosen as the smallest ridge width.

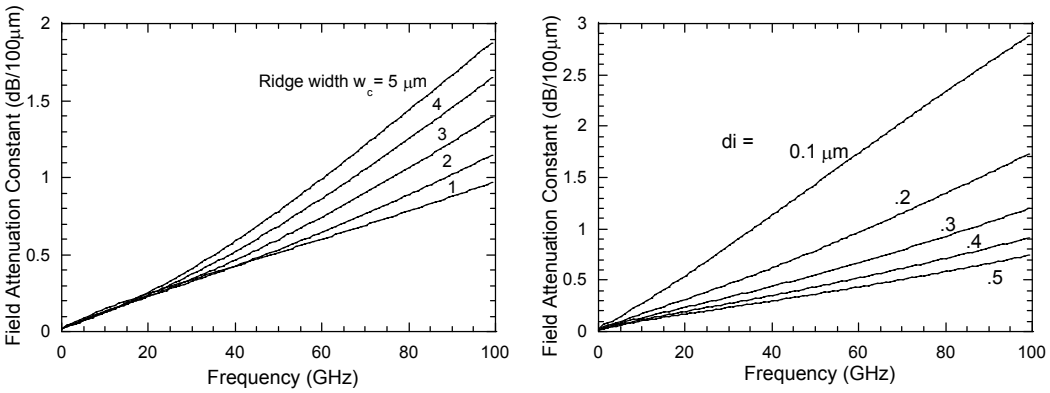

Figure 6. Field attenuation with different waveguide width and intrinsic region thickness.

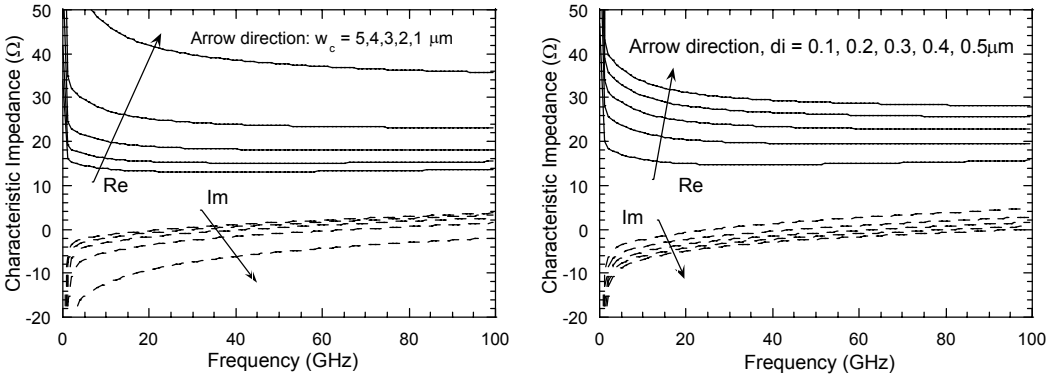

Figure 7. Characteristic impedance with different ridge widths (a) and different intrinsic region.

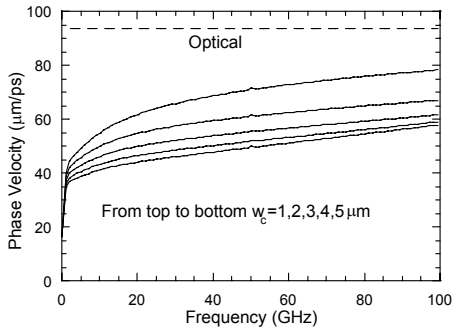

Figure 8. Phase velocity calculated as a function of frequency for different ridge widths.

Figure 8 shows the calculated phase velocity of microwave for different ridge widths, (the active thickness is 300nm). For different widths, the microwave velocity is about two third of the optical velocity. The walk-off time difference for the two waves to pass the device will be about 2.5ps. Considering a device of length 300μm, the bandwidth limitation is about 100GHz. Even though the group velocities can be a little bit different from the phase velocities, we can still conclude that the group velocity mismatch limited bandwidth will be much higher than the range we are considering (DC to 50 GHz). Based on this reason, the design will mostly focus on reducing the microwave loss at high frequencies, either by reducing the reflection loss, or by reducing the propagation loss.

2.2 Two port transmission and distributed EO response

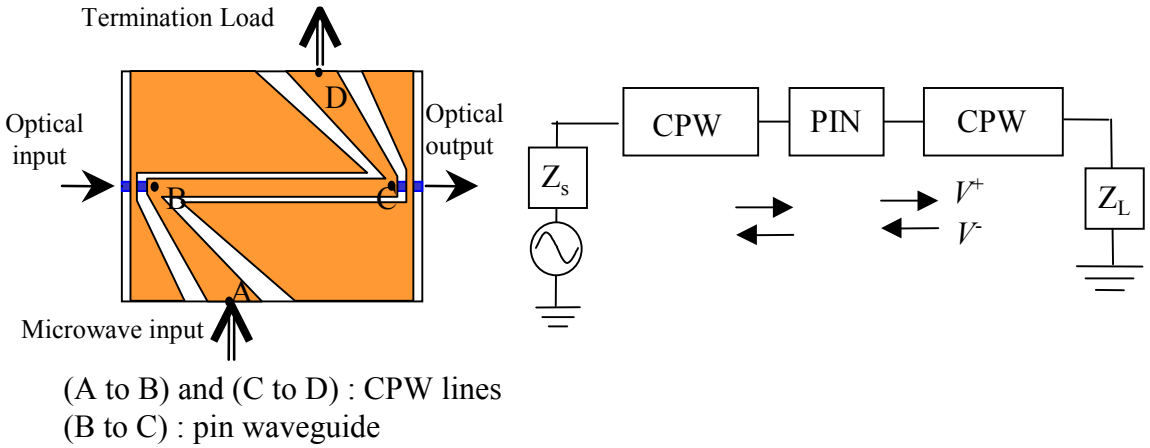

Figure 9. Schematic diagram of device, which is composed by waveguide (p-i-n) and two CPW lines. The distributed voltage is calculated by the two-port transmission matrix method, while the voltage V is the phasor in frequency domain.

Practically, the device needs CPW lines for electrical source feeding and termination. Figure 9 shows the schematic diagram of device. To calculate microwave propagation along the whole structure, two port linear transmission matrix is used [9]. The device is separated into three sections, CPW feed line and loaded line (AB, and CD in figure 9) and the waveguide section (BC). Each section can be model as a linear two-port network with a transmission matrix. In the matrix, the electrical wave is composed of a forward and backward wave. As the electric propagation characteristics are calculated by the methods of section 2.1 with the source and loaded terminations, the electric amplitude and phase distribution with space can be extracted. Therefore, once the termination is decided the voltage distribution on each point of the waveguide can be determined.

The time-dependent optical output intensity, $P(t)$, can be expressed by

$$P(t) = A \cdot [\exp(-\alpha_o L - \int_0^L \Delta\bar{k}(z, t' + t - \frac{L}{v_o}) \cdot dz)]$$
$$\Delta\bar{k}(z,t) = \Delta\alpha(z,t) + j \cdot \Delta n(z,t) \cdot k_o \qquad (1)$$
$$z = v_o \cdot t'; j = \sqrt{-1}; k_o = 2\pi / \lambda_o$$

where the factor A includes the optical input power intensity and the fiber coupling losses at both ends, v_0 is the optical group velocity, α_o is the optical loss at zero bias, L is the waveguide length, λ_o is the optical wavelength, and t' is the time for the optical wave to travel from the input to position z. The voltage-dependent optical wave number, $\Delta\bar{k}(z,t)$, comprises the real part, $\Delta\alpha(z,t)$, which is the modal absorption coefficient change due to the electroabsorption effect, and the imaginary part, $\Delta n(z,t) \cdot k_0$, which is the phase change originating from the Kramers-Kronig relation. To extract the modal absorption coefficient and phase change, some basic D.C. optical transmission and chirp measurement are used[10].

Equation (1) reveals the distributed effects of EO-conversion on the microwave propagation. At each point, z , along the waveguide, electroabsorption takes place only with the simultaneously applied voltage. Therefore, once the timely micrwave signal and bias voltage are obtained, the output optical power with time can be extracted. By this model, the effects of velocity mismatch, microwave loss and termination can be calculated.

3. DEVICE FABRICATION AND MEASUREMENT

The material was grown on a semi-insulating InP substrate. The active region (MQW) is sandwiched by n- and p- InP layers, where n-InP is the bottom layers (0.5μm thick) and p-InP is the top layers (1.7μm thick). The MQWs were designed for polarization insensitive operation, where tensile-strain was used in the quantum well and the barrier is

compressively-strained which compensates the well so that the total thickness of MQW can be grown thick without misfit dislocation. The InGaAsP well has –0.37% tensile strain with thickness 10.4nm and the barrier has +0.5% compressive strain with thickness 7.6nm. The active region includes 11 barriers and 10 quantum wells. A commercial software is used to simulate the absorption spectra [11]. In unstrained quantum wells, the light hole has a larger transition energy to the conduction band than the heavy hole, due to the smaller effective mass. Therefore, the absorption edge for the TM polarization mode is at higher photon energies than that of the TE mode. To achieve identical transition energies, the light hole band gap is reduced by applying tensile strain. The resulting absorption in our quantum well is shown in Fig. 10 for both polarization modes.

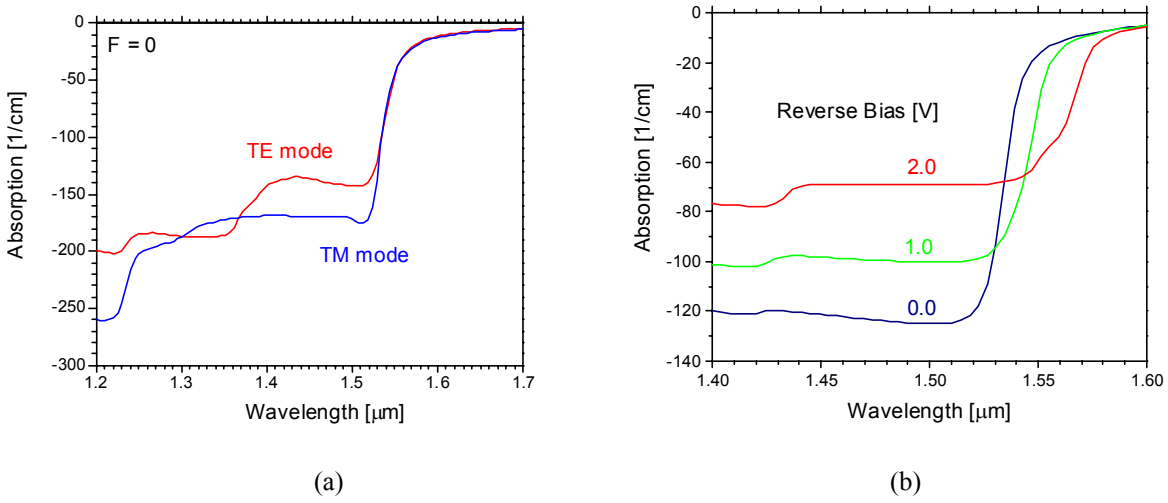

Figure 10. (a) Calculated absorption spectra for TE and TM mode with zero field. (b) Calculated absorption spectra for increasing bias (TE).

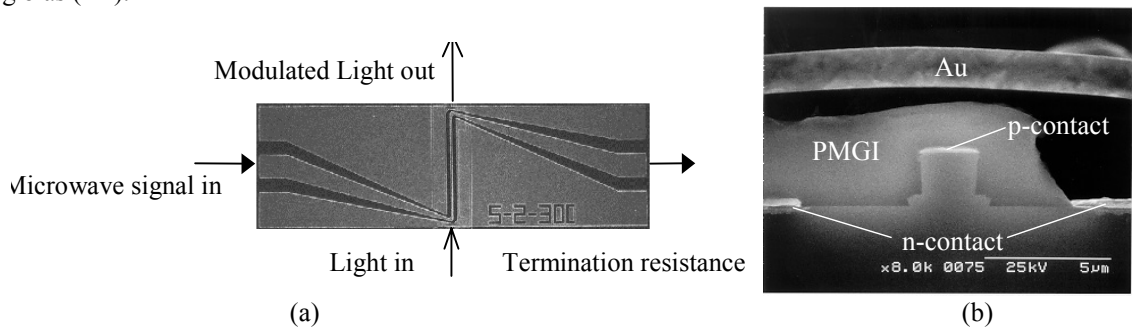

Figure 11. (a) Top view of device. (b) Facet of waveguide.

The device is fabricated by general p-i-n ridge waveguide processing. The p-contact layer (Ti/Pt/Au) was evaporated by lift-off processing. Following the p-metal mask, CH_4/ H_2/Ar reactive ion etching (RIE) was used to define the ridge waveguide under *insitu* laser monitoring the surface. Waveguide width is 2μm. After dry etching, the n-contact layer (Ni/AuGe/Ni/Au) was deposited. Both p- and n- contacts were treated by rapid-thermal-annealing at 410^0C for about 30 seconds. PMGI was then spun for etching surface passivation and planarization, while O_2 plasma was used to etch the PMGI for the metal bridge. A 2μm thick Ti/Au is used to form CPW line. The top and facet views of the device are shown in the figure 11. After cleaving, the facet was anti-reflection coated.

Figure 12 shows the microwave characteristics with frequency, which is extracted from the S-matrix network analyzer. The results are in agreement with the calculated data of figure 6 and figure 7. Due to the highly loaded intrinsic capacitance, this kind of slow waveguides suffer from the highly lossy propagation, dispersion, and lower impedance. The loss is about 0.5dB per 100μm long device, limiting the length of the device. Also, the absolute impedance is about 25Ω, which is much lower than instrument impedance 50Ω. Figure 13 shows the device S11 and S12 at open, short and 50Ω termination. The calculated data (line curves) are consistent with the experiment data (dot curves). S11s are quite sensitive

to the output termination, indicating that the output loaded impedance should be engineered to diminish the reflection at the output. With the S12 measurement for 50Ω load, there is about –6dB loss at 40GHz, where the single trip loss is about 1.5dB (figure 12). It suggests that the high impedance mismatch on the input and output will give excess loss. The dashed curve of figure 13(b) is the calculation based on the RC-lump type. The difference from the measurement suggests that the port-to-port transmission is based on the wave phenomena, especially at high frequency.

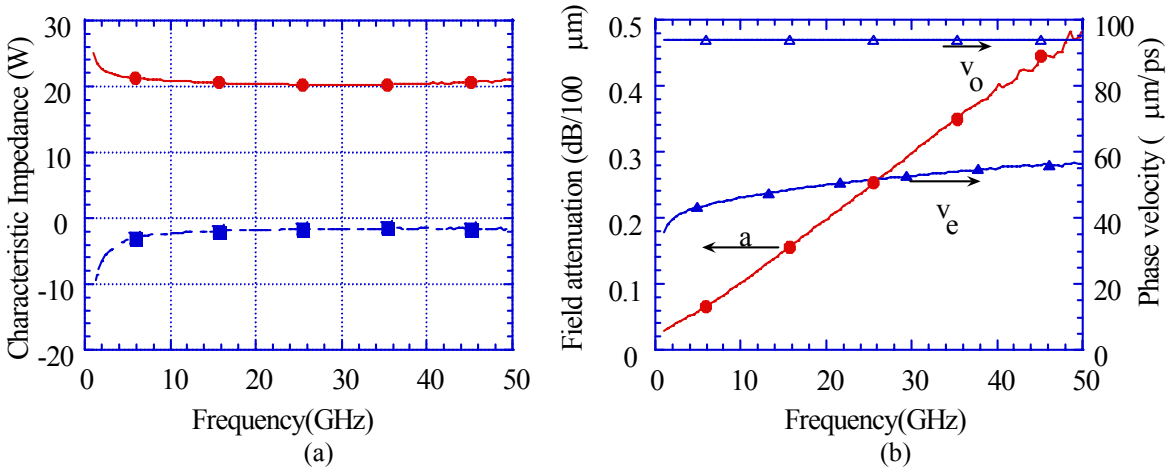

Figure 12. Microwave characteristics of the waveguide, (a) characteristic impedance. (b) microwave attenuation and phase velocity, top curve is the optical velocity.

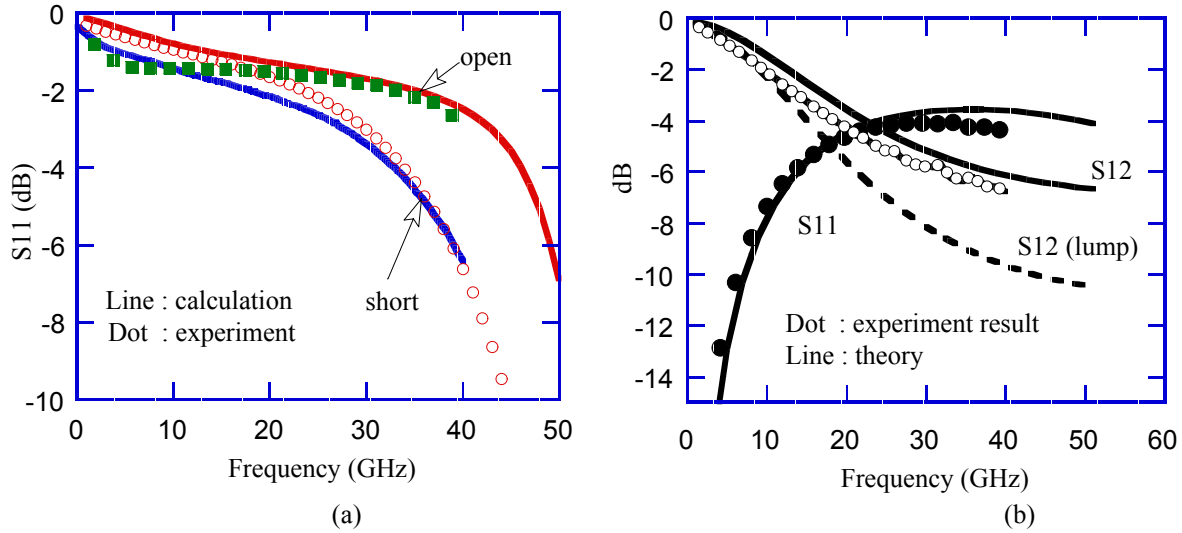

Figure 13. S11 and S12 for different terminations, (a) open and short cases. (b) the 50Ω case. The dash curve of (b) is the calculation result based on the lump-type.

Fig. 14(a) shows the fiber-to-fiber optical transmission versus reverse bias voltage for several wavelengths and for TE and TM polarization states. The device length was 300μm, and the ridge width was 2 μm. With TE polarization, the drive voltage for 10-dB extinction ratio was 0.8 V and it was 1.2 V for a 20-dB extinction ratio at 1550 nm. Little dependence on polarization is observed due to the strained quantum well design. It should be noted that the drive voltage for 20-dB extinction ratio was 1.28 V for TM polarization.

The EO-conversion effects are shown in the figure 14(b). HP Lightwave component network analyzer was used. The dots are for the measurements and the curves are for the theoretical calculations. Without any load termination, the 3-dB bandwidth was about 10.7 GHz. It increased to 18 GHz with a 50 Ω termination from the output cascade probe. When a thin film resistor with impedance of 35 Ω was used to terminate the output port via a ribbon bond, the bandwidth exceeded 20 GHz. An extrapolated bandwidth from the theoretical prediction was 24.7 GHz, yielding to a figure of merit of 17.2 GHz/V for this device. The key feature on the response curve with 35-Ω termination was the resonance peak, which was

mainly caused by the microwave reflections at the load and the source ends and at the interfaces between the optical waveguide and the feed lines. Because of the negative reflection at the load, the response at some frequencies was enhanced. This effect was also observed in traveling-wave electro-optic modulators [12]. For comparison, as shown in figure15, 500μm long devices with traveling wave and lump type devices were fabricated. The bandwidth of traveling type is about 22.5 GHz. The drop of relative EO response is about 0.7 dB more than the one of 300μm (as shown in figure14). It is mainly from the microwave loss and velocity mismatch in the long device. The field attenuation at 20 GHz is about 0.2 dB/100μm, so the corresponding excess loss for 200um more length of transmission is about 0.4dB. Furthermore, the lump type devices (bottom two curves of figure 15) shows higher penalty on bandwidth than the top curve, indicating the advantage of traveling structures.

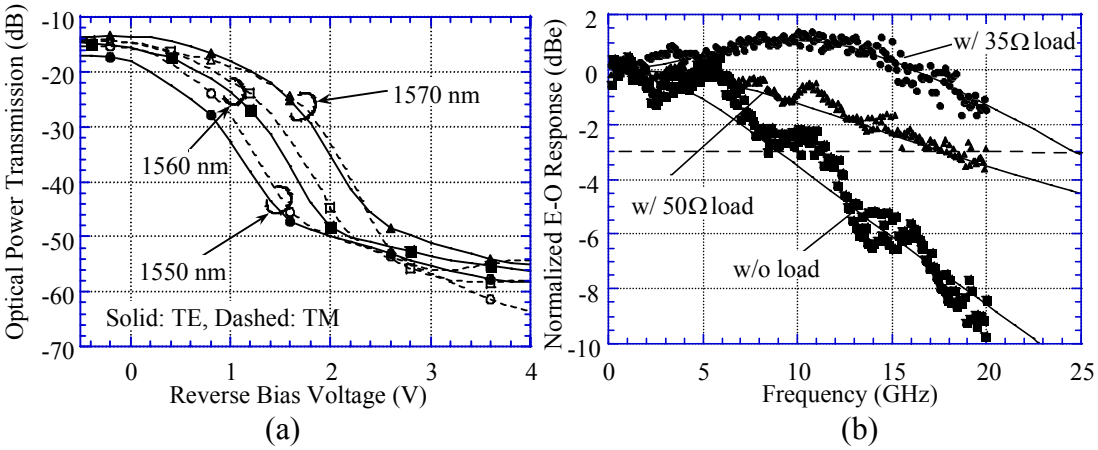

Figure 14. (a) Optical transmission with different bias. (b) Normalized electrical-to-optical response under different terminations. The solid curve is the calculated results.

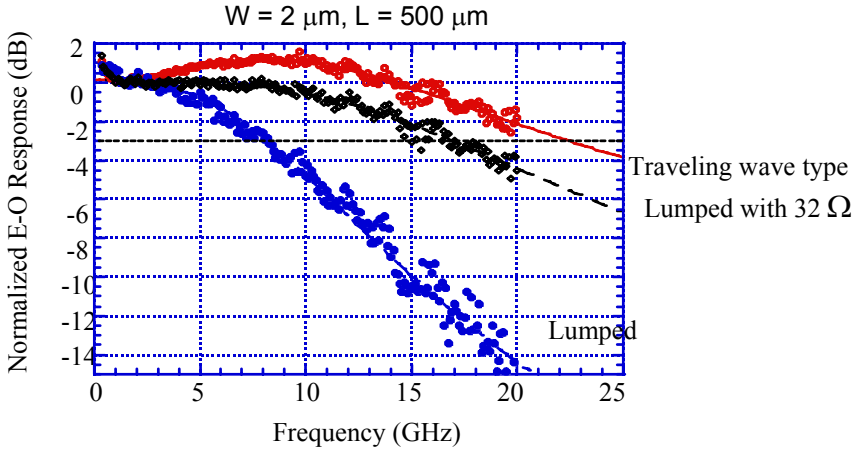

Figure 15. EO response for 500 μm long device. The bottom two curves are from the Lump type device (left of figure 2) of same length.

Driving sinusoidal electrical signals on EAMs to generate optical short pulses [12-14] has been widely used for optical-time-division-multiplexing (OTDM) systems. For high speed OTDM system, the requirements for optical short pulses are high extinction ratio, high average power, short pulses. The EAMs fitting these requirement should have high speed EO-response, high on-off ratio at low driving voltage (>30dB) and high optical output power (>-25dBm) on 30GHz [12]. With two long TWEAMs (300μm and 400μm), the walk-off time (~7ps 700μm transmission) between optical and microwave is high. The tandem TWEAMs were thus used. As shown in figure16 (a), after two TWEAM transmission, the optical transmission experiences higher than 45dB on-off ratio and the modulation efficiency is above 25dB per voltage. In figure 16(b), the pulse widths generated by single ones has broaden pulses, however, tuning the phase between two microwaves applied on the tandem structure results in the maximum optical output power and high extinction ratio. A pulse below 4.5 ps can be obtained with high average power. The line curves of figure 16(b) are the calculated results based on

the distributed effects. The calculation fits the experiment results, suggesting that the TWEAM structures are useful for fast switching widow in OTDM.

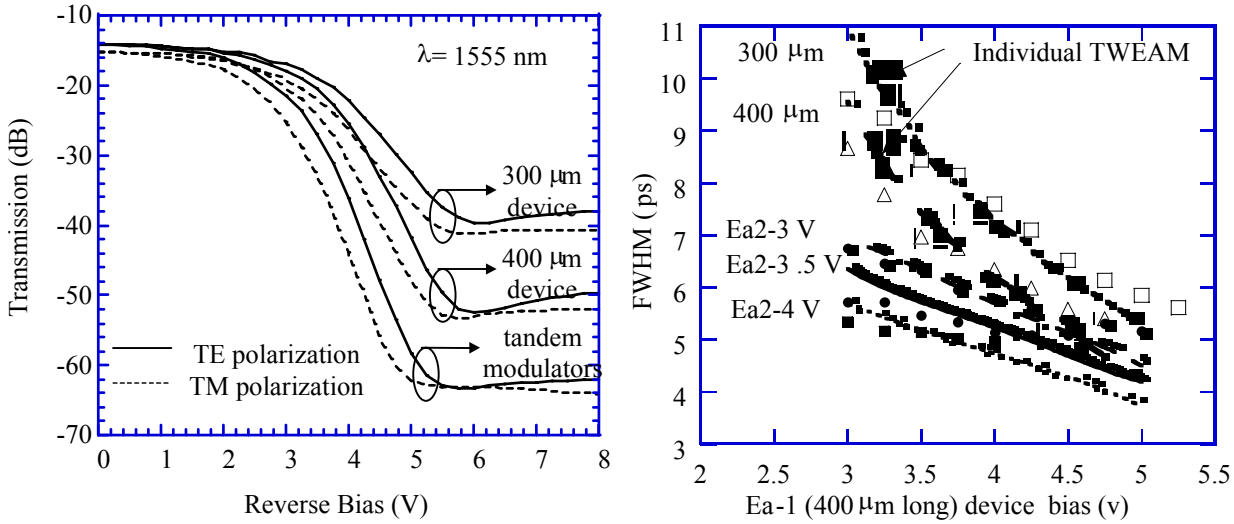

(a) (b)

Figure 16. (a) Tandem TWEAM D.C. optical transmission with bias. (b) Optical short pulse generated by 30GHz sinusoidal electrical signal, single and tandem. The line curves are the theoretical results.

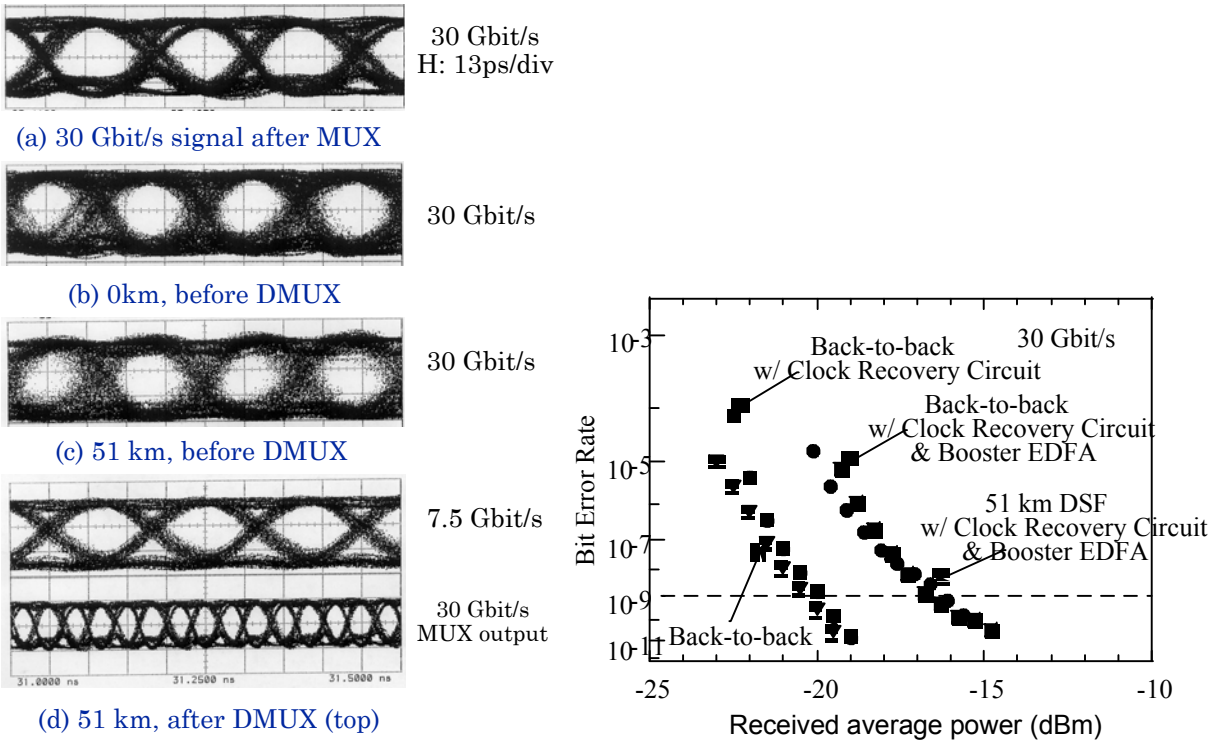

Figure 17. (left) 30 Gbit/s eye diagrams of (a) the output signal from the 4:1 MUX, the received signal after transmission through (b) 0 km and (c) 51 km dispersion shifted fiber. The top half of Fig. (d) is the DMUX output after 51-km transmission, and the bottom half is the MUX output (right), bit error testing at 30Gbit/s.

To further examine the device performance, a 300μm TWEAM was used in 30Gbit/s non-return-to-zero NRZ transmission measurement. An electrical 30Gbits/s data was generated by multiplexing four 7.5 Gbits/s signals. After

transmission, the data was 1:4 demultiplexed to four 7.5 Gbits/s signals. As shown in figure 17, the eye diagrams show similar patterns even after 51km, and the bit-error-rate test after 51km indicate that the power penalty for the error floor is due to the noise of EDFA. The successful NRZ data transmission at 30GHz verifies that the TWEAM has a broad bandwidth performance over 30GHz.

4. SUMMARY

Traveling wave electroabsorption modulators using the quantum confined Stark effect in InGaAsP multiple quantum wells (MQWs) have been demonstrated. Low drive voltage (above 20dB/V), high extinction ratio (above 40dB for on-off ratio), and a modulation bandwidth higher than 20GHz have been demonstrated. Limitations of the high-speed performance of TWEAMs arise mostly from microwave propagation loss and the low characteristic impedance. By using integrated tandem TWEAMs to adjust the microwave phase between two modulators, an optical switch window (< 4.5 ps) is demonstrated. Due to the broad-band performance above 20GHz, successful data transmission experiments at 30 Gbit/s have shown a promising system performance with these devices.

5. REFERENCES

[1] G. Bastard, E. E. Mendez, L. L. Chang, and L. Esaki, "Variational calculations on a quantum well in an electric field," *Phys. Rev. B, Condens. Matter*, vol. 28, pp. 3241-3245, 1983.

[2] S. Nojima, Y. Kawaguchi, K. Nakashima, and K. Wakita, "Field-induced energy shift of excitonic absorption in InGaAs/InP multiquantum wells grown by metalorganic molecular beam epitaxy," *Jpn. J. Appl. Phys. 2, Lett.*, vol. 26, pp. 1927-1928, 1987.

[3] S. Nojima, Y. Kawamura, K. Wakita, and O. Mikami, "Electric field effects in excitonic absorption for high-quality InGaAs/InAlAs multiple-quantum-well structures," *J. Appl. Phys.*, vol. 64, pp. 2795-2797, 1988.

[4] S. Nojima and K. Wakita, "Optimization of quantum well materials and structures for excitonic electroabsorption effects," *Appl. Phys. Lett.*, vol. 53, pp. 1958-1960, 1988.

[5] Ido, T.; Tanaka, S.; Suzuki, M.; Koizumi, M.; Sano, H.; Inoue, H. Ultra-high-speed multiple-quantum-well electro-absorption optical modulators with integrated waveguides. Journal of Lightwave Technology, vol.14, (no.9), IEEE, Sept. 1996 p.2026-34.

[6] Kawano, K.; Kohtoku, M.; Ueki, M.; Ito, T.; Kondoh, S.; Noguchi, Y.; Hasumi, Y. "Polarisation-insensitive travelling-wave electrode electroabsorption (TW-EA) modulator with bandwidth over 50 GHz and driving voltage less than 2 V". Electronics Letters vol.33, (no.18), IEE, 28 Aug. 1997. p.1580-1.

[7] Zhang, C.Z.; Yi-Jen Chiu; Abraham, P.; Bowers, J.E. "25 GHz polarization-insensitive electroabsorption modulators with traveling-wave electrodes". IEEE Photonics Technology Letters, vol.11, (no.2), IEEE, Feb. 1999. p.191-3.

[8] K. S. Giboney, J. W. Rodwell, and J. E. Bowers, "Traveling-wave photodetector theory," *IEEE Trans. Microw. Theory Tech.* , vol. 45, pp. 1310-1319, 1997.

[9] R.E. Collin, Foundation for Microwave Engineering. McGraw-Hill Book Company.

[10] F. Dorgeuille and F. Devaux, " On the transmission performance and the chirp parameter of a multiple-quantum-well electroabsorption modulator,", IEEE J.Quantum Electronic., vol30,pp2565,1994.

[11] APSYS by Crosslight Software

[12] Kaman, V.; Yi-Jen Chiu; Liljeberg, T.; Zhang, S.Z.; Bowers, J.E. "Integrated tandem traveling-wave electroabsorption modulators for >100 Gbit/s OTDM applications". IEEE Photonics Technology Letters, vol.12, (no.11), IEEE, Nov. 2000. p.1471-3.

[13] Moodie, D.G.; Harlow, M.J.; Guy, M.J.; Perrin, S.D.; Ford, C.W.; Robertson, M.J. "Discrete electroabsorption modulators with enhanced modulation depth". Journal of Lightwave Technology, vol.14, (no.9), IEEE, Sept. 1996. p.2035.

[14] Souli, N.; Ramdane, A.; Devaux, F.; Ougazzaden, A.; Slempkes, S. "Tandem of electroabsorption modulators integrated with a DFB laser and an optical amplifier for short optical pulse generation and coding". IEE Proceedings-Optoelectronics, vol.145, (no.3), IEE, June 1998. p.198-204.

[15] S. Y. Wang and S. H. Lin, "High speed III-V electrooptic waveguide modulators at λ=1.3 μm," *J. Lightwave Technol.*, vol. 6, pp. 758-771, 1988.